

Not So Black? The Statistics of Albedo and Energy Recirculation on Hot Exoplanets

Nicolas B. Cowan¹, Eric Agol¹,

Received _____; accepted _____

¹Astronomy Department, University of Washington, Box 351580, Seattle, WA 98195
email: cowan@astro.washington.edu agol@astro.washington.edu

ABSTRACT

Spectroscopic and photometric observations of short-period exoplanets have led to a wide variety of numerical models for terminator absorption spectra, day-side emission spectra, and disc-averaged photometric light curves. In contrast to those —often underconstrained— simulations, we use a simple analytic model to analyze *all* of the published photometric observations of exoplanets. Our model has two parameters: the planets’ Bond albedo, A , and its heat recirculation efficiency, ε . We demonstrate how different kinds of observations (reflected eclipse, thermal eclipse and phase variation) constrain A and ε . By combining the published observations for 20 exoplanets, we confirm that no single combination of albedo and recirculation efficiency fit all short-period planets. We then allow each planet to have a unique A and ε , and construct a two-dimensional distribution function for the albedo and recirculation efficiency of short-period planets. The only region of the A - ε plane that is *not* populated is $A > 0.9$. The variety of recirculation efficiencies has been widely discussed, but the large range of best-fit albedos in our models is surprising. Part of the high- A distribution stems from degeneracies in the observations and from small-number statistics, but we also suggest two physical explanations. Firstly, the day-side brightness temperature of the planets exhibits a sharp rise from near-infrared to optical wavelengths. This is to be expected if either a) the optical observations are probing layers of the planet’s atmosphere that are hotter than its effective temperature, which should be true by definition; and/or b) reflected light is contributing to the observed secondary eclipse depth. Secondly, some planets that have published thermal eclipse *and* phase variations, have energy budgets that require significant albedo. Either way, fully half of our sample have best-fit albedos *greater* than $A = 0.5$, implying that the very low albedo of HD 209458 ($A < 0.1$, Rowe et al. 2008)

may not be the norm. If this is the case, NASA’s Kepler mission should observe many eclipses and phase variations of short-period planets in *reflected* rather than thermal light.

Subject headings: methods: data analysis — (stars:) planetary systems —

1. Introduction

Short-period exoplanets¹ are expected to have atmospheric compositions and dynamics completely different from Solar System giant planets. These planets orbit $\sim 100\times$ closer to their host stars than Jupiter is from the Sun. As a result, they receive $\sim 10^4\times$ more flux and experience tidal forces $\sim 10^6\times$ stronger than Jupiter. In contrast to Jupiter, which releases as much power in its interior as it receives from the Sun, short-period exoplanets have atmospheres controlled by their host stars.

There is a growing body of data that constrain what short-period planets look like. Observations of secondary eclipses, starting with Deming et al. (2005) and Charbonneau et al. (2005), have made it possible to measure the integrated day-side flux of short-period exoplanets. To characterize planets’ longitudinal temperature profiles, observations have been made at a variety of points in the planet’s orbit. Observations with low signal-to-noise, due either to infrequent time sampling (Harrington et al. 2006; Cowan et al. 2007) or large photometric uncertainties (Snellen et al. 2009a; Borucki et al. 2009; Knutson et al. 2009b), have been used to create two-hemisphere models of planets. When the signal-to-noise is high, it is possible to use light curve inversion (Cowan & Agol 2008) to produce rough longitudinal maps of planets (Knutson et al. 2007a, 2009c).

It has been pointed out (e.g., Harrington et al. 2006; Cowan et al. 2007) that observations of secondary eclipses and phase variations constrain a combination of a planet’s Bond albedo, A , and its recirculation efficiency, ε (also parametrized as f or P_n , Guillot et al. 1996; Burrows et al. 2006). At thermal wavelengths (where most of these

¹For our purposes a “short period” exoplanet is one where the periastron distance is less than 0.1 AU, regardless of its actual period. They are all Class IV and V extrasolar giant planets in the scheme of Sudarsky et al. (2003).

observations have been taken), albedo and recirculation both have the effect of decreasing the day-side brightness. At shorter wavelengths, reflected starlight begins to dominate, so observations are primarily sensitive to albedo.

In § 2 we introduce a simple model to quantify the day-side and night-side energy budget of a short-period planet, and show how the model parameters, A and ε , can be constrained by observations. In § 3 we use all the published observations to obtain best-fit values of A and ε . We discuss our results in § 4 and state our conclusions in § 5.

2. Toy Model of Energy Budget

Short-period planets have an energy budget entirely dictated by the flux they receive from their host star, which dwarfs tidal heating or remnant heat of formation. Following Hansen (2008), we define the equilibrium temperature at the planet’s sub-stellar point: $T_0(t) = T_{\text{eff}}(R_*/r(t))^{1/2}$, where T_{eff} and R_* are the star’s effective temperature and radius, and $r(t)$ is the planet–star distance (for a circular orbit r is simply equal to the semi-major axis, a). What a planet does with the flux that it receives depends on its albedo, A , and recirculation efficiency, ε .

Secondary eclipse occurs at superior conjunction, when we are seeing the planet’s day-side. At that point in the orbit the planet–star distance is $r_{\text{sc}} = a(1-e^2)/(1+e \cos(3\pi/2-\omega))$, where e and ω are the planet’s orbital eccentricity and argument of periastron, respectively. At secondary eclipse, and in the absence of energy circulation, the equilibrium temperature depends on the normalized projected distance, γ , from the center of the planetary disc as $T_{\text{eq}} = T_0(1 - \gamma^2)^{1/8}$. The thermal secondary eclipse depth in this limit is given by:

$$\frac{F_{\text{day}}}{F_*} \Big|_{\text{therm}} = \left(\frac{R_p}{R_*} \right)^2 \left(\frac{hc}{\lambda k T_0} \right)^8 (e^{hc/\lambda k T_b} - 1) \times \int_0^{(\lambda k T_0/hc)^8} \frac{dx}{\exp(x^{-1/8}) - 1}, \quad (1)$$

where T_b is the brightness temperature of the star at wavelength λ .

In the $\varepsilon = 0$ limit, then, the day-side emergent spectrum is not exactly that of a blackbody, even if each annulus *does* have a blackbody spectrum. The differences are not important at the level of the present study, however. By integrating Equation 1 over λ (see also Burrows et al. 2008; Hansen 2008), one obtains the effective temperature of the day-side in the no-albedo, no-recirculation limit: $T_{\text{day}} = (2/3)^{1/4}T_0$. Indeed, treating the planet’s day-side as a uniform hemisphere emitting at this temperature gives nearly the same wavelength dependence as the more complex Equation 1.

By the same token, we can express the day-side brightness temperature in the limit of uniform day-side temperature and $T = 0$ on the night-side (this is often referred to as the planet’s “equilibrium temperature”): $T_{\text{day}} = (1/2)^{1/4}T_0$, and in the limit of a uniform temperature throughout the planet: $T_{\text{day}} = (1/4)^{1/4}T_0$.

Comparing the day-side brightness temperatures in the three limits of circulation above leads to the following simple parametrization of the day-side temperature in terms of the planetary albedo and recirculation efficiency:

$$T_{\text{day}}(A, \varepsilon) = T_0(1 - A)^{1/4} \left(\frac{2}{3} - \frac{5}{12}\varepsilon \right)^{1/4}, \quad (2)$$

where the energy circulation is $0 < \varepsilon < 1$. Note that our definition of ε is nearly identical to the Burrows et al. (2006) definition of P_n . Our $\varepsilon = 0$ limit produces a hotter day-side brightness than the $P_n = 0$ limit, however, and our parameter runs from 0 to 1 rather than from 0 to 0.5.

By the same token, we can parametrize the night-side temperature as:

$$T_{\text{night}}(A, \varepsilon) \approx T_0(1 - A)^{1/4} \left(\frac{\varepsilon}{4} \right)^{1/4}. \quad (3)$$

Note that T_{day} and T_{night} are the equator-weighted temperatures of their respective hemispheres. As such, they will tend to be slightly higher than the hemisphere-averaged

temperature, except in the $\varepsilon = 1$ limit. This is also why the quantity $T_{\text{day}}^4 + T_{\text{night}}^4$ is still a weak function of ε : at high recirculation efficiencies some of the absorbed stellar flux is advected or diffuses towards the poles.

The secondary eclipse depth, including reflected and emitted light, is given by:

$$\frac{F_{\text{day}}}{F_*} = A \frac{2}{3} \left(\frac{R_p}{r_{\text{sc}}} \right)^2 + \left(\frac{R_p}{R_*} \right)^2 \frac{e^{hc/\lambda k T_b} - 1}{e^{hc/\lambda k T_{\text{day}}} - 1}. \quad (4)$$

Since phase variations have so far only been published for planets with circular orbits, we only need an expression for the day–night brightness contrast in that (much simpler) case:

$$\frac{F_{\text{day}} - F_{\text{night}}}{F_*} = \frac{F_{\text{day}}}{F_*} - \left(\frac{R_p}{R_*} \right)^2 \frac{e^{hc/\lambda k T_b} - 1}{e^{hc/\lambda k T_{\text{night}}} - 1}. \quad (5)$$

2.1. How Observations Constrain A and ε

The secondary eclipse depth at optical wavelengths is dominated by reflected light, and is therefore a direct measurement of the planet’s albedo. The amplitude of phase variations in reflected light does not yield any additional information, since the night-side of a planet does not reflect any light (by definition).

A measurement of the thermal secondary eclipse depth for a planet can be thought of as a measurement of the planet’s brightness factor, $0 < \beta < 1$, the ratio of the planet’s day-side brightness temperature to its fiducial temperature at superior conjunction:

$$\beta = \frac{T_{\text{day}}}{T_0} = (1 - A)^{1/4} \left(\frac{2}{3} - \frac{5}{12} \varepsilon \right)^{1/4}. \quad (6)$$

The night-side brightness of the planet places a constraint on $0 < \nu < 4^{-1/4}$:

$$\nu = \frac{T_{\text{night}}}{T_0} = (1 - A)^{1/4} \left(\frac{\varepsilon}{4} \right)^{1/4}. \quad (7)$$

The thermal phase variation constrains the difference between the day-side and night-side flux of the planet. The amplitude, $0 < \alpha < 1$, of the phase variations in the Rayleigh-Jeans tail is:

$$\alpha = \frac{T_{\text{day}} - T_{\text{night}}}{T_0} = \beta - \nu. \quad (8)$$

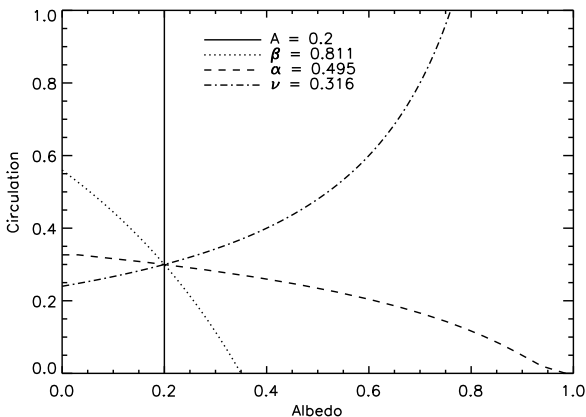


Fig. 1.— Different kinds of observations constrain the albedo, A and recirculation efficiency, ε , differently. A measurement of the secondary eclipse depth at optical wavelengths is purely a measure of albedo (solid line). A secondary eclipse depth at thermal wavelengths gives a joint constraint on albedo and recirculation (dotted line). Thermal phase variations also give a joint constraint on the two variables, but are better at measuring circulation (dashed line). An independent measurement of the night-side brightness yields a constraint (the dot-dashed line) nearly orthogonal to the day-side measurement.

In Figure 1 we show how different kinds of observations constrain A and ε . In all cases we chose a constraint consistent with $A = 0.2$ and $\varepsilon = 0.3$. The solid line is a locus of constant A ; the dotted line is the locus of constant β ; the dashed line is a locus of constant α ; the dot-dashed line is a locus of constant ν . From this figure it is clear that the measurements complement each other, but the combination of optical eclipse and thermal phase variations is the most potent (since the solid and dashed lines are nearly

perpendicular).

3. Analysis

3.1. Planetary & Stellar Data

Table 1. Secondary Eclipses & Phase Variations of Exoplanets

Planet	T_0 (K) ^a	λ (μm)	Eclipse Depth ^b	T_{day} (K) ^c	Phase Amplitude ^b	A	ε	χ^2
51 Peg b ¹	1944	8	N/A	N/A	$< 7 \times 10^{-4}$ (2σ)	N/A	N/A	
τ Bootis b ²	2308	0.48	N/A	N/A	$< 5 \times 10^{-5}$ (1σ)	N/A	N/A	
ν Andromeda b ³	2572	24	N/A	N/A	$2.9(7) \times 10^{-3}$	< 0.23	< 0.02	0.5
CoRoT-1b ⁴	2682	0.6	$1.6(6) \times 10^{-4}$	2736(117)	N/A	0.00(2)	0.00(4)	10.5
		0.71	$1.26(33) \times 10^{-4}$	2409(75)	$1.0(3) \times 10^{-4}$			
		2.095	$2.8(5) \times 10^{-3}$	2738(125)	N/A			
		2.147	$3.36(42) \times 10^{-3}$	2532(159)	N/A			
CoRoT-2b ⁵	2173	0.6	$6(2) \times 10^{-5}$	2324(75)	N/A	0.18(3)	0.3(2)	8.4
		0.71	$1.02(20) \times 10^{-4}$	2212(47)	N/A			
		4.5	$5.10(42) \times 10^{-3}$	1851(73)	N/A			
		8	$4.1(1.1) \times 10^{-3}$	1325(193)	N/A			
Gl 436b ⁶	1040	8	$5.7(8) \times 10^{-4}$	810(45)	N/A	0.3(3)	0.4(4)	0
		8	$5.4(7) \times 10^{-4}$	793(40)	N/A			
Gl 876d ⁷	966	8	N/A	N/A	$< 5.13 \times 10^{-5}$ (3σ)	N/A	N/A	
HAT-P-1b ⁹	1829	3.6	$8.0(8) \times 10^{-4}$	1418(47)	N/A	0.0(2)	0.6(4)	3.0
		4.5	$1.35(22) \times 10^{-3}$	1505(101)	N/A			
		5.8	$2.03(31) \times 10^{-3}$	1620(127)	N/A			
		8.0	$2.38(40) \times 10^{-3}$	1571(156)	N/A			
HAT-P-7b ⁸	3017	0.65	$1.30(11) \times 10^{-4}$	3033(35)	$1.22(16) \times 10^{-4}$	0.55(4)	0.0(1)	8.3
		3.6	$9.8(1.7) \times 10^{-4}$	2062(158)	N/A			
		4.5	$1.59(22) \times 10^{-3}$	2368(180)	N/A			
		5.8	$2.45(31) \times 10^{-3}$	2857(242)	N/A			
		8	$2.25(52) \times 10^{-3}$	2490(410)	N/A			
HD 80606b ¹⁰	1991	8	$1.36(18) \times 10^{-3}$	1144(76)	N/A	0.6(2) ^d	1.0(5)	0
HD 149026b ¹¹	2469	8	$8.4(1.2) \times 10^{-4}$	N/A ^e	N/A	0.7(2)	0.3(2)	0
		8	$3.7(0.8) \times 10^{-4}$	1581(203)	$2.3(7) \times 10^{-4}$			
HD 179949b ¹²	2197	8	N/A	N/A	$1.41(33) \times 10^{-3}$	< 0.45	< 0.23	0
HD 189733b ¹³	1730	3.6	$2.56(14) \times 10^{-3}$	1638(34)	N/A	0.24(3)	0.67(3)	103
		4.5	$2.14(20) \times 10^{-3}$	1316(46)	N/A			
		5.8	$3.10(34) \times 10^{-3}$	1365(69)	N/A			
		8	$3.381(55) \times 10^{-3}$	1254(11)	N/A			
		8	$3.91(22) \times 10^{-3}$	1356(42)	$1.2(2) \times 10^{-3}$			

Table 1—Continued

Planet	T_0 (K) ^a	λ (μm)	Eclipse Depth ^b	T_{day} (K) ^c	Phase Amplitude ^b	A	ε	χ^2
HD 209458b ¹⁴	1933	16	$5.51(30) \times 10^{-3}$	1339(53)	N/A			
		24	$5.98(38) \times 10^{-3}$	1302(66)	N/A			
		24	$5.36(27) \times 10^{-3}$	1193(47)	$1.3(3) \times 10^{-3}$			
		0.5	$7(9) \times 10^{-6}$	2333(243)	N/A	0.04(5)	0.63(9)	34
		2.2	$< 3 \times 10^{-4}(1\sigma)$	< 1463	N/A			
		3.6	$9.4(9) \times 10^{-4}$	1447(47)	N/A			
		4.5	$2.13(15) \times 10^{-3}$	1756(57)	N/A			
		5.8	$3.01(43) \times 10^{-3}$	1894(151)	N/A			
		8	$2.40(26) \times 10^{-3}$	1488(93)	$< 1.5 \times 10^{-3} (2\sigma)$			
24	$2.60(44) \times 10^{-3}$	1127(148)	N/A					
OGLE-TR-56b ¹⁵	3196	0.9	$3.63(91) \times 10^{-4}$	2700(114)	N/A	0.4(4)	0.4(4)	0
OGLE-TR-113b ¹⁶	1899	2.2	$1.7(5) \times 10^{-3}$	1908(158)	N/A	0.0(1)	0.0(1)	1.2
TrES-1b ¹⁷	1635	3.5	$< 1.5 \times 10^{-3}(1\sigma)$	< 1500	N/A	0.4(2)	1.0(5)	3.1
		4.5	$6.6(1.3) \times 10^{-4}$	972(56)	N/A			
		8	$2.25(36) \times 10^{-3}$	1157(93)	N/A			
TrES-2b ¹⁸	2115	3.6	$1.27(21) \times 10^{-3}$	1492(86)	N/A	0.0(3)	0.9(5)	3.5
		4.5	$2.30(24) \times 10^{-3}$	1646(76)	N/A			
		5.8	$1.99(54) \times 10^{-3}$	1374(173)	N/A			
8	$3.59(60) \times 10^{-3}$	1665(169)	N/A					
TrES-3b ¹⁹	2339	2.2	$2.41(43) \times 10^{-3}$	2099(115)	N/A	0.7(1)	0.0(3)	16
		3.6	$3.46(35) \times 10^{-3}$	1815(74)	N/A			
		4.5	$3.72(54) \times 10^{-3}$	1648(106)	N/A			
		5.8	$4.49(97) \times 10^{-3}$	1618(179)	N/A			
		8	$4.75(46) \times 10^{-3}$	1475(83)	N/A			
TrES-4b ²⁰	2480	3.6	$1.37(11) \times 10^{-3}$	1886(63)	N/A	0.6(3)	0.0(5)	5.8
		4.5	$1.48(16) \times 10^{-3}$	1725(85)	N/A			
		5.8	$2.61(59) \times 10^{-3}$	2101(279)	N/A			
		8	$3.18(44) \times 10^{-3}$	2174(204)	N/A			
WASP-12b ²¹	3644	0.9	$8.2(1.5) \times 10^{-4}$	2997(104)	N/A	0.5(5)	0.5(5)	0
XO-1b ²²	1710	3.6	$8.6(7) \times 10^{-4}$	1300(33)	N/A	0.5(3)	0.0(4)	8.7
		4.5	$1.22(9) \times 10^{-3}$	1263(34)	N/A			
		5.8	$2.61(31) \times 10^{-3}$	1545(91)	N/A			

We begin by considering all the published photometric observations of exoplanets, summarized in Table 1. We discard τ -Bootis b, 51 Peg b and Gl 876d, since they are non-transiting planets for which only an upper limit on the phase variations was measured. This leaves us with 20 exoplanets for which there are useful constraints on A , ε , or both. The two remaining non-transiting planets in our sample, ν -Andromeda b and HD 179949b, are useful because they exhibit thermal phase variations, which place a lower limit on α . To be able to directly compare these planets to their transiting counterparts, however, it is necessary to assume a planetary radius and an orbital inclination: we use $R_p = 1.2R_J$ and an edge-on inclination. Clearly the orbital inclination can not be exactly edge-on, since the planet would then transit its star. This assumption, however, gives the most conservative (lowest) constraints on α .

Stellar and planetary data are taken from exoplanet.eu, maintained by Jean Schneider, and references therein. When the stellar data are not available, we have assumed typical parameters for the appropriate spectral class, and solar metallicity. Insofar as we are only concerned with the broadband brightnesses of the stars, our results should not depend sensitively on the input stellar parameters. Using the stars' T_{eff} , $\log g$ and $[\text{Fe}/\text{H}]$, we use the PHOENIX/NextGen stellar spectrum grids (Hauschildt et al. 1999) to determine their brightness temperatures at the observed bandpasses². For each waveband for which eclipse or phase observations have been obtained, we determine the ratio of the stellar flux to the blackbody flux at that grid star's T_{eff} . We then apply this factor to the T_{eff} of the observed star.

It is significant that the choice of stellar model leads to systematic uncertainties in the planetary brightness that are of order the photometric uncertainties. For example, Christiansen et al. (2009) use stellar models for HAT-P-7 from Kurucz (2005), while we

²The model spectra are available at <http://www.hs.uni-hamburg.de/EN/For/ThA/phoenix/index.html>

Table 1—Continued

Planet	T_0 (K) ^a	λ (μm)	Eclipse Depth ^b	T_{day} (K) ^c	Phase Amplitude ^b	A	ϵ	χ^2
XO-2 ²³	1861	8	$2.10(29) \times 10^{-3}$	1213(87)	N/A			
		3.6	$8.1(1.7) \times 10^{-4}$	1446(103)	N/A	0.6(3)	0.0(5)	1.9
		4.5	$9.8(2.0) \times 10^{-4}$	1336(103)	N/A			
		5.8	$1.67(36) \times 10^{-3}$	1495(157)	N/A			
		8	$1.33(49) \times 10^{-3}$	1173(220)	N/A			

^aThe equilibrium temperature at the sub-stellar point during superior conjunction.

^bEclipse depths and phase amplitudes are unitless, since they are measured relative to stellar flux.

^cThe day-side brightness temperature at a given wavelength. Note that at short wavelengths, this number has no bearing on the actual temperature of the planet, but rather is a measure of the planet’s albedo.

^dThis planet is on a highly eccentric orbit, with superior conjunction occurring just before periastron, so the low day-side brightness temperature may have nothing to do with low albedo. Rather, the absorbed stellar flux is probably stirring up winds that have died down during the 100+ days far the star.

^eA re-analysis of the Harrington et al. (2007) data indicates a much smaller eclipse depth consistent with subsequent observations (Knutson et al. 2009b). We therefore ignore the original published depth in our analysis.

¹Cowan et al. (2007), ²Charbonneau et al. (1999), ³Harrington et al. (2006), ⁴Snellen et al. (2009a); Alonso et al. (2009b); Gillon et al. (2009a); Rogers et al. (2009), ⁵Alonso et al. (2009a); Snellen et al. (2009b); Gillon et al. (2009b), ⁶Deming et al. (2007b); Demory et al. (2007), ⁷Seager & Deming (2009), ⁸Todorov et al. (2010), ⁹Borucki et al. (2009); Christiansen et al. (2009), ¹⁰Laughlin et al. (2009), ¹¹Harrington et al. (2007); Knutson et al. (2009b), ¹²Cowan et al. (2007), ¹³Deming et al. (2006); Knutson et al. (2007a); Charbonneau et al. (2008); Knutson et al. (2009c), ¹⁴Richardson et al. (2003); Deming et al. (2005); Cowan et al. (2007); Rowe et al. (2008); Knutson et al. (2008), ¹⁵Sing & López-Morales (2009), ¹⁶Snellen & Covino (2007), ¹⁷Charbonneau et al. (2005); Knutson et al. (2007b), ¹⁸O’Donovan et al. (2009), ¹⁹Fressin et al. (2009), ²⁰Knutson et al. (2009a), ²¹Lopez-Morales et al. (2009), ²²Machalek et al. (2008), ²³Machalek et al. (2009)

use those of Hauschildt et al. (1999). The resulting 8 μm brightness temperatures for HAT-P-7b differ by as much as 600 K, or slightly more than 1σ .

3.2. Brightness Temperature vs Effective Temperature

The planet’s albedo and recirculation efficiency govern its effective day-side and night-side temperatures, $T_{\text{eff,day}}$ and $T_{\text{eff,night}}$, respectively. Observationally, we can only measure the brightness temperature, ideally at a number of different wavelengths: $T_{\text{bright}}[\lambda_i]$. If one knew, *a priori*, the emergent spectrum of a planet, one could trivially convert a single brightness temperature to an effective temperature. Alternatively, if observations were obtained at a number of wavelengths near the planet’s blackbody peak, it would be possible to empirically estimate the planet’s bolometric flux and hence its effective temperature. Unfortunately, most observations to date have been obtained at mid-IR wavelengths, on the R-J tail for short-period planets.

Hot exoplanets without stratospheric inversions should have nearly isothermal temperature profiles near the day-side IR photosphere. The highest brightness temperatures should therefore occur in opacity windows, where the photosphere is the deepest and hottest. Planets with temperature inversions, on the other hand, should show high temperatures in the high opacity regions of the spectrum, where one is probing the hot stratosphere. In spectral regions with low opacity (a.k.a. “windows”) one may probe the temperature minimum near the tropopause, yielding lower brightness temperatures. Because of these nuances, the brightness temperature is not always a good estimate of the planet’s effective temperature.

Numerical simulations of hot exoplanet emergent spectra (e.g., Seager et al. 2005; Burrows et al. 2008) offer insight to how T_{bright} might differ from T_{eff} . In the Rayleigh-Jeans

tail, the spectrum is relatively smooth and T_{eff} tends to be slightly higher than T_{bright} . On the Wien tail and near the peak, the spectrum may look like a picket fence if the optical opacity is much lower than the infrared opacity. In this case, the planet’s T_{eff} will lie between the brightness temperature of the windows and that of the troughs.

Our approach amounts to setting T_{eff} equal to the weighted mean of the observed brightness temperatures, with an uncertainty determined by the scatter in $T_{\text{bright}}[\lambda_i]$. In cases where only a single observation have been published, we set the uncertainty equal to the published uncertainty in the brightness temperature. We treat each observation as an entirely independent constraint that produces a χ^2 surface of its own. The joint constraint from all of the observations for a given planet is obtained by summing these individual χ^2 surfaces.

3.3. Populating the A - ε Plane

For each planet we calculate eclipse depths and phase variation amplitudes on a 50×50 grid in albedo, A , and circulation efficiency, ε , for all wavelengths at which the planet has been observed. At each grid point we compute the χ^2 by comparing the model eclipse depths and phase amplitudes to their observed counterparts. As pointed out in Madhusudhan & Seager (2009), there are often fewer data than there are model parameters, so we cannot use the usual degrees-of-freedom or reduced χ^2 to quantify goodness-of-fit³.

The best-fit solution is simply the grid point with the smallest χ^2 . The 1σ confidence

³Note that with 2 parameters we require 3 data for a given planet to have a sensibly constrained model. This means that 7 of the 20 planets in our sample are underconstrained, even with our spartan model. To put this in perspective, Madhusudhan & Seager (2009) have 9 model parameters.

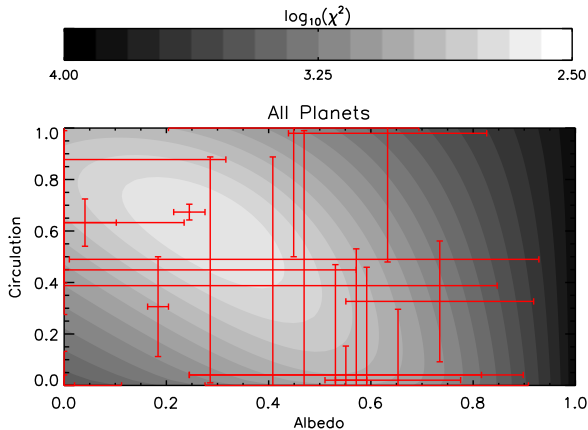


Fig. 2.— The χ^2 surface for short-period exoplanets in the A - ε plane. The gray-scale shows the sum of the χ^2 surfaces for all 20 planets, but is dominated by HD 189733b ($A = 0.2$, $\varepsilon = 0.7$), which benefits from the most numerous and highest signal-to-noise observations. The red points show the best-fit parameters and associated 1σ uncertainties for each planet.

interval is defined as those grid points for which the χ^2 is within 1 of the minimum. We construct a normalized probability surface $P \propto e^{-\chi^2/2}$ for each planet, then multiply these together to create the gray-scale in Figure 2. The goodness-of-fit for a single set of parameters over all exoplanets is poor: the best χ^2 is $10^{2.59} \approx 389$, the degrees of freedom are $71 - 2 = 69$, for a reduced χ^2 of 5.6. Understandably, the χ^2 surface is largely governed by HD 189733b and HD 209458b, the two most-studied transiting exoplanets. The poor fit of a single (A, ε) tells us that (1) the planets have heterogeneous properties, and/or (2) the planets have severely non-blackbody emergent spectra, and/or (3) the observational uncertainties have been under-estimated.

If we don't require all the planets to have the same albedo and recirculation, we can instead create a probability distribution for the heterogeneous population of short-period exoplanets. We create a two-dimensional normalized probability distribution function (PDF) for each planet, then add these together to create the global PDF shown in Figure 3.

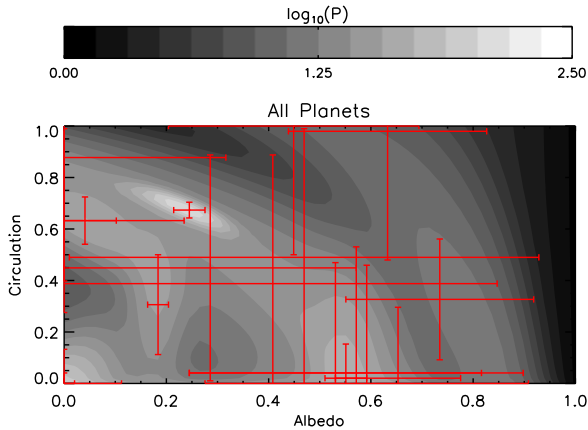


Fig. 3.— The global distribution function for short-period exoplanets in the A - ε plane. The gray-scale shows the sum of the normalized probability distribution function for all 20 planets. The red points show the best-fit parameters and associated 1σ uncertainties for each planet.

This is more democratic way of representing the data, since each planet’s distribution contributes as much. The global PDF is still dominated by the few very-well characterized planets, but only because they have the most peaked distributions.

The distribution in Figure 3 appears bimodal in night-side temperature, ν , with a cluster of planets with high ε and low A , and another with low ε and high A . This apparent bimodality arises because most of the observational constraints are secondary eclipses at thermal wavelengths (typically with the IRAC camera on *Spitzer*; Werner et al. 2004; Fazio et al. 2004), which exhibit an A - ε degeneracy (see the dotted line in Figure 1). In other words, most exoplanet observations are of the planets’ day-side, so it is understandable that there are large uncertainties in the night-side temperature.

In Figures 4 and 5 we show the distribution functions for the albedo and circulation of the 20 planets in our sample. While a simple histogram (shown with the dotted lines) shows strongly bimodal distributions for both parameters, the more careful analysis shown

by the solid lines —marginalizing the global PDF of Figure 3 over either A or ε — yields much more uniform distributions. The dashed line in Figure 4 shows the ε -distribution if one requires the albedo to be low, $A < 0.2$. There are then many high-recirculation planets, since advection is the only way to depress the day-side temperature in the absence of albedo. Forcing the albedo to be this low results in a large increase in χ^2 , however.

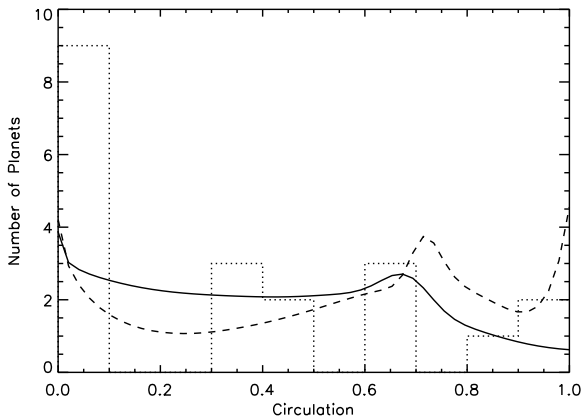


Fig. 4.— The solid black line shows the projection of the 2-dimensional probability distribution function (the gray-scale of Figure 3) projected onto the ε -axis. The dotted line shows a simple histogram of the best-fit circulation efficiencies (the red points from Figure 3). The bimodality is questionable, but the distribution is very broad, regardless of how one constructs the distribution. The dashed line shows the ε -distribution if one requires that all planets have albedos less than 20%.

4. Discussion

4.1. Recirculation Efficiency

The first few measurements of hot Jupiter phase variations showed signs that these planets are not all cut from the same cloth. Harrington et al. (2006) and Knutson et al.

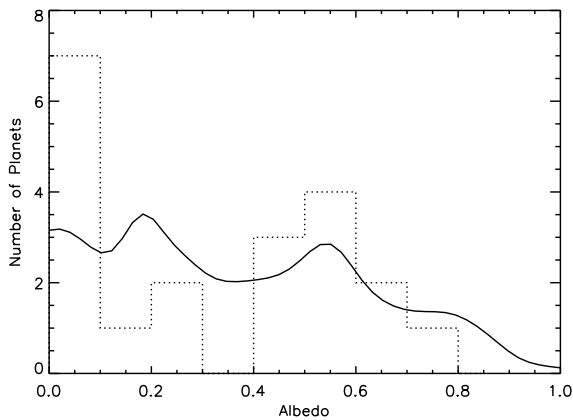


Fig. 5.— The solid black line shows the projection of the 2-dimensional probability distribution function (the gray-scale of Figure 3) projected onto the A -axis. The dotted line shows a simple histogram of the best-fit albedos (the red points from Figure 3). The bimodality is questionable, but the distribution is very broad, regardless of how one constructs the distribution.

(2007a) quoted very different phase function amplitudes for the ν Andromeda and HD 189733 systems. It was not clear whether the differences were intrinsic to the planets, however, because the data were taken with different instruments, at different wavelengths, and with very different observation schemes. The uniform study presented in Cowan et al. (2007), however, showed that HD 179949b and HD 209458b exhibit significantly different degrees of energy recirculation, confirming prior suspicions.

The presence or lack of a stratospheric temperature inversion on the day-sides of exoplanets has been invoked to explain the purported bimodality in recirculation efficiency on hot Jupiters (Hubeny et al. 2003; Fortney et al. 2006, 2008; Burrows et al. 2007, 2008; Zahnle et al. 2009). The argument, simply put, is that optical absorbers high in the atmosphere of extremely hot Jupiters would absorb incident photons where the radiative timescales are short, making it difficult for these planets to recirculate energy (i.e., keeping

ε low). The most robust detection of this temperature inversion is for HD 209458b (Knutson et al. 2008), but this planet does not exhibit a large day-night brightness contrast at $8 \mu\text{m}$ (Cowan et al. 2007).

Looking at the solid line in Figure 4, the bimodality in ε is dubious, though there is a wide range of behaviors. If stratospheric temperature inversions play a role in determining the energy circulation efficiency on short-period planets it must do so in a more gradual way. If exoplanets have uniformly low albedos, then many planets are perfectly efficient at redistributing absorbed stellar flux (dashed line in Figure 4).

4.2. Albedo

Since the astonishing measurements of HD 209458b taken with the Canadian MOST satellite (Rowe et al. 2008), it has been taken for granted that all short-period planets have albedos on par with that of charcoal ($\sim 5\%$). Figure 5 shows that this consensus may be premature. More than half of the planets in our sample (11 of 20) have best-fit $A > 0.4$.

To better understand why our model requires significant albedos for some planets, it is useful to define $\beta_{obs} = T_{day}/T_0$, where T_{day} is the observed day-side brightness temperature from a secondary eclipse measurement. The secondary eclipse depth (SED) divided by the transit depth (TD) is a direct measure of the ratio of the planet’s day-side intensity to the star’s intensity $\psi = B_{day}/B_*$. In the Rayleigh-Jeans tail, the expression reduces to $\psi = T_{day}/T_b$. Knowing the star’s brightness temperature at a given wavelength, it is possible to compute the apparent brightness temperature of the planet’s day side:

$$T_{day} = \frac{hc}{\lambda k} \left[\log \left(1 + \frac{e^{hc/\lambda k T_b} - 1}{\psi} \right) \right]^{-1}, \quad (9)$$

where T_b is the star’s brightness temperature at the given wavelength.

Formally, the uncertainty in β_{obs} is a combination of the uncertainties in the secondary

eclipse and transit depths, as well as uncertainties in the star’s brightness and effective temperatures. In practice, the eclipse depth uncertainty, σ_{SED} , usually dominates the error budget:

$$\sigma_{\beta} \approx \left(\frac{\sigma_{SED}}{T_0 \times \text{TD}} \right) \left| \frac{\partial T_{\text{day}}}{\partial \psi} \right|, \quad (10)$$

where

$$\frac{\partial T_{\text{day}}}{\partial \psi} = T_{\text{day}}^2 \frac{\lambda k}{hc} \left(\frac{e^{hc/\lambda k T_b} - 1}{\psi^2 + \psi(e^{hc/\lambda k T_b} - 1)} \right). \quad (11)$$

In the case of a distant system, the uncertainty in the star’s effective and brightness temperatures can be quite large: OGLE-TR-113 has an effective temperature of 4800 ± 150 K. We have neglected this contribution in our analysis, so our uncertainties are —if anything— an underestimate.

In Figure 6 we show the distribution of β_{obs} , the observed day-side brightness temperature normalized by the substellar equilibrium temperature during superior conjunction. We treat each secondary eclipse measurement as a normalized Gaussian centered on the associated β_{obs} and with a width proportional computed according to Equation 10. The distribution function is constructed by adding together these Gaussian functions. If all the planets in our sample had zero albedo and emitted like blackbodies, the distribution should lie between the red dotted and solid lines. Most of the observations brighter than the $A = 0, \varepsilon = 0$ limit (red solid line) were obtained at short wavelengths, where reflected light should start contributing (contrast the solid and dashed black lines).

In Figure 7 we show how the observed day-side brightness temperature varies with wavelength. We have normalized the wavelength by the peak wavelength for a planet at T_0 ($\lambda/\lambda_{\text{peak}} < 1$ are on the Wein tail; $\lambda/\lambda_{\text{peak}} = 1$ at the peak; $\lambda/\lambda_{\text{peak}} > 1$ on the Rayleigh-Jeans tail). The downturn in β_{obs} at long wavelengths is likely due to the fact that the emergent spectrum of hot Jupiters exhibits $T_{\text{bright}} < T_{\text{eff}}$ in the Rayleigh-Jeans tail. There appears to be an upturn in the distribution at short wavelengths, which one would

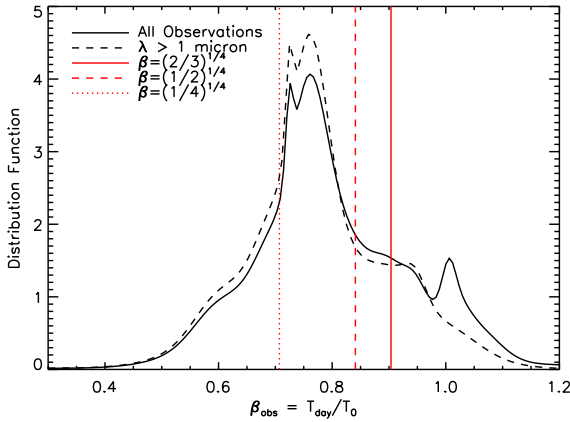


Fig. 6.— The distribution of β_{obs} , the observed brightness temperature normalized by the substellar equilibrium temperature during superior conjunction. At thermal wavelengths $\beta_{obs} = \beta$, described in Equation 6, but at short wavelengths the brightness begins to be contaminated—and eventually dominated—by reflected light. The solid black line shows the distribution for all the secondary eclipse observations. The dashed black line shows the distribution after removing observations shortward of 1 micron, which may include reflected light. The red lines correspond to three fiducial limits of recirculation, assuming $A = 0$: no recirculation (solid), uniform day-hemisphere (dashed), and uniform planet (dotted).

expect if reflected light was contaminating the eclipse depths. This explains some of the high- A from our analysis.

Alternatively, the emissivity of the planets may be greater at optical wavelengths than at mid-IR wavelengths, in agreement with realistic spectral models of hot Jupiters, which predict brightness temperatures greater than T_{eff} on the Wien tail (e.g., Seager et al. 2005). Note that this increase in emissivity should occur regardless of whether or not the planet has a stratosphere: by definition, the depth at which the optical thermal emission is emitted is the depth at which incident starlight is absorbed, which will necessarily be a hot layer. We can naively estimate the maximum temperature of this layer as $(2/3)^{1/4}T_0$, the effective

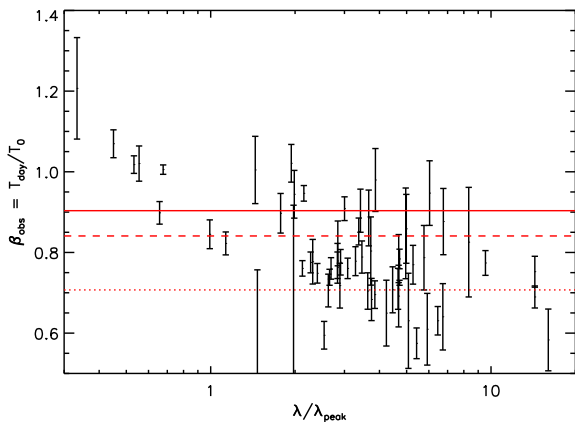


Fig. 7.— The observed day-side brightness temperature normalized by the sub-stellar equilibrium temperature in the $A = 0$, $\varepsilon = 0$ limit, plotted against the unitless wavelength of the observation (the wavelength of the observation normalized by the peak wavelength for T_0). All published secondary eclipse observations are shown. The red lines correspond to three fiducial limits of recirculation, assuming $A = 0$: no recirculation (solid), uniform day-hemisphere (dashed), and uniform planet (dotted). The up-turn at short wavelengths may be due to reflected light, a rise in emissivity, or both. The drop-off at long wavelengths may be indicating that the brightness temperatures on the R-J tail are below the effective temperature.

day-side temperature in the $A = 0$, $\varepsilon = 0$ limit. The up-turn in β_{obs} shown in in Figure 7 may be too high to be due to this opacity effect alone, but an analysis involving model spectra is beyond the scope of this paper (and in any case such analyses have already been performed elsewhere).

An independent way to get leverage on A is to look at planets for which both thermal eclipses and phase variations have been observed: HD 149026b, HD 189733b, and HD 209458b. As shown by the dashed and dotted lines in Figure 1, this combination—though not ideal—gives some leverage on albedo. In particular, a planet with a shallow

thermal eclipse and relatively large thermal phase variations is indicative of a planet with a relatively large albedo: If the energy is not being radiated away on the day-side *or* the night-side, it must have been reflected away in the first place. Our best-fit albedo for HD 149026b is $A = 0.7 \pm 0.2$, and for HD 189733b is $A = 0.20 \pm 0.03$.

5. Conclusions

In summary, the combination of optical observations of secondary eclipses and thermal observations of phase variations is the best way to constrain planetary albedo and circulation. No planet has yet been characterized in this way. The optical observations should be taken near the star’s blackbody peak, both to maximize signal-to-noise, and to avoid contamination from the planet’s thermal emission. The thermal observations, likewise, should be near the planet’s blackbody peak to better constrain its bolometric flux. Note that this wavelength is shortward of the ideal contrast ratio, which typically falls on the planet’s Rayleigh-Jeans tail.

At present, short-period planets appear to populate nearly the entire A – ε plane. This is likely due to observational uncertainties and degeneracies. But even the three planets with the best constraints differ significantly from one another (see Table 1): CoRoT-1b has low albedo and low recirculation (in good agreement with Rogers et al. 2009), HD 209458b has low albedo and high recirculation (as in Cowan et al. 2007), HD 189733b has moderate albedo and high recirculation, HAT-P-7b has high albedo and low recirculation (the inefficient recirculation is unanimous, but the high albedo is in stark contrast to the interpretation of Christiansen et al. 2009). If this heterogeneity is typical of short-period exoplanets, NASA’s Kepler mission should observe many eclipses and phase variations in reflected light (i.e., in systems where the planet’s blackbody peak is well outside Kepler’s sensitivity range).

Our best-fit albedo for HD 189733b is $20 \pm 3\%$ and for TrES-3b is $70 \pm 10\%$, so precise photometry of these systems at visible wavebands (with either HST or large ground-based telescopes) should reveal a secondary eclipse in reflected light at the level of 10^{-4} . HAT-P-7b and CoRoT-1b should both exhibit large infrared phase variations, since both planets have cool night-sides, according to our study and others. The Warm *Spitzer* mission should be able to verify this behavior at 3.6 and 4.5 μm (Deming et al. 2007a).

In this study, we have treated the day and night-side of short-period exoplanets as uniform blackbodies. While this approximation is not correct in detail, it allows us to compare all the varied observations of these planets to one another, and to draw conclusions about the entire population of planets. If our predictions are born out, it will indicate that the blackbody approximation still has its place in comparative exoplanetology. If, however, these predictions do not pan out, it will indicate that a more complex analysis needs to be carried out to be able to compare the disparate observations in a meaningful way.

The current paucity of detailed observations means that detailed physical simulations are necessarily under-constrained. As more eclipse and phase observations are published, however, it will become worthwhile to use a more sophisticated analytic model (see, for example, § 4.2 of Hansen 2008) to interpret the data. At this stage, most planets have only been observed in the four IRAC bandpasses, and the uncertainties are often large enough to admit a single brightness temperature, making it difficult to pin down even our modest two model parameters.

A possible improvement to this study would be to redo the data reduction for the *Spitzer* exoplanet observations of hot Jupiters. These data make up the majority of the constraints presented in our study and most are publicly available. And while the published observations were analyzed in disparate ways, a consensus approach to correcting detector systematic is beginning to emerge.

The authors acknowledge useful discussions of spectroscopy with T. Robinson. N.B.C. was supported by the Natural Sciences and Engineering Research Council of Canada. E.A. is supported by a National Science Foundation Career Grant. Support for this work was provided by NASA through an award issued by JPL/Caltech.

REFERENCES

- Alonso, R. et al. 2009a, *A&A*, 506, 353
- Alonso, R., Guillot, T., Mazeh, T., Aigrain, S., Alapini, A., Barge, P., Hatzes, A., & Pont, F. 2009b, *A&A*, 501, L23
- Borucki, W. J. et al. 2009, *Science*, 325, 709
- Burrows, A., Budaj, J., & Hubeny, I. 2008, *ApJ*, 678, 1436
- Burrows, A., Hubeny, I., Budaj, J., Knutson, H. A., & Charbonneau, D. 2007, *ApJ*, 668, L171
- Burrows, A., Sudarsky, D., & Hubeny, I. 2006, *ApJ*, 650, 1140
- Charbonneau, D. et al. 2005, *ApJ*, 626, 523
- Charbonneau, D., Knutson, H. A., Barman, T., Allen, L. E., Mayor, M., Megeath, S. T., Queloz, D., & Udry, S. 2008, *ApJ*, 686, 1341
- Charbonneau, D., Noyes, R. W., Korzennik, S. G., Nisenson, P., Jha, S., Vogt, S. S., & Kibrick, R. I. 1999, *ApJ*, 522, L145
- Christiansen, J. L. et al. 2009, ArXiv e-prints
- Cowan, N. B., & Agol, E. 2008, *ApJ*, 678, L129
- Cowan, N. B., Agol, E., & Charbonneau, D. 2007, *MNRAS*, 379, 641
- Deming, D., Agol, E., Charbonneau, D., Cowan, N., Knutson, H., & Marengo, M. 2007a, in *American Institute of Physics Conference Series*, Vol. 943, American Institute of Physics Conference Series, ed. L. J. Storrie-Lombardi & N. A. Silbermann, 89–100

- Deming, D., Harrington, J., Laughlin, G., Seager, S., Navarro, S. B., Bowman, W. C., & Horning, K. 2007b, *ApJ*, 667, L199
- Deming, D., Harrington, J., Seager, S., & Richardson, L. J. 2006, *ApJ*, 644, 560
- Deming, D., Seager, S., Richardson, L. J., & Harrington, J. 2005, *Nature*, 434, 740
- Demory, B.-O. et al. 2007, *A&A*, 475, 1125
- Fazio, G. G. et al. 2004, *ApJS*, 154, 10
- Fortney, J. J., Cooper, C. S., Showman, A. P., Marley, M. S., & Freedman, R. S. 2006, *ApJ*, 652, 746
- Fortney, J. J., Lodders, K., Marley, M. S., & Freedman, R. S. 2008, *ApJ*, 678, 1419
- Fressin, F., Knutson, H. A., Charbonneau, D., O'Donovan, F. T., Burrows, A., Deming, D., & Mandushev, G. 2009, ArXiv e-prints
- Gillon, M. et al. 2009a, *A&A*, 506, 359
- . 2009b, ArXiv e-prints
- Guillot, T., Burrows, A., Hubbard, W. B., Lunine, J. I., & Saumon, D. 1996, *ApJ*, 459, L35+
- Hansen, B. M. S. 2008, *ApJS*, 179, 484
- Harrington, J., Hansen, B. M., Luszcz, S. H., Seager, S., Deming, D., Menou, K., Cho, J. Y.-K., & Richardson, L. J. 2006, *Science*, 314, 623
- Harrington, J., Luszcz, S., Seager, S., Deming, D., & Richardson, L. J. 2007, *Nature*, 447, 691
- Hauschildt, P. H., Allard, F., & Baron, E. 1999, *ApJ*, 512, 377

- Hubeny, I., Burrows, A., & Sudarsky, D. 2003, *ApJ*, 594, 1011
- Knutson, H. A., Charbonneau, D., Allen, L. E., Burrows, A., & Megeath, S. T. 2008, *ApJ*, 673, 526
- Knutson, H. A. et al. 2007a, *Nature*, 447, 183
- Knutson, H. A., Charbonneau, D., Burrows, A., O’Donovan, F. T., & Mandushev, G. 2009a, *ApJ*, 691, 866
- Knutson, H. A., Charbonneau, D., Cowan, N. B., Fortney, J. J., Showman, A. P., Agol, E., & Henry, G. W. 2009b, *ApJ*, 703, 769
- Knutson, H. A. et al. 2009c, *ApJ*, 690, 822
- Knutson, H. A., Charbonneau, D., Deming, D., & Richardson, L. J. 2007b, *PASP*, 119, 616
- Kurucz, R. L. 2005, *Memorie della Societa Astronomica Italiana Supplement*, 8, 14
- Laughlin, G., Deming, D., Langton, J., Kasen, D., Vogt, S., Butler, P., Rivera, E., & Meschiari, S. 2009, *Nature*, 457, 562
- Lopez-Morales, M., Coughlin, J. L., Sing, D. K., Burrows, A., Apai, D., Rogers, J. C., & Spiegel, D. S. 2009, *ArXiv e-prints*
- Machalek, P., McCullough, P. R., Burke, C. J., Valenti, J. A., Burrows, A., & Hora, J. L. 2008, *ApJ*, 684, 1427
- Machalek, P., McCullough, P. R., Burrows, A., Burke, C. J., Hora, J. L., & Johns-Krull, C. M. 2009, *ApJ*, 701, 514
- Madhusudhan, N., & Seager, S. 2009, *ApJ*, 707, 24

- O’Donovan, F. T., Charbonneau, D., Harrington, J., Seager, S., Deming, D., & Knutson, H. A. 2009, in IAU Symposium, Vol. 253, IAU Symposium, 536–539
- Richardson, L. J., Deming, D., & Seager, S. 2003, ApJ, 597, 581
- Rogers, J. C., Apai, D., López-Morales, M., Sing, D. K., & Burrows, A. 2009, ApJ, 707, 1707
- Rowe, J. F. et al. 2008, ApJ, 689, 1345
- Seager, S., & Deming, D. 2009, ApJ, 703, 1884
- Seager, S., Richardson, L. J., Hansen, B. M. S., Menou, K., Cho, J. Y.-K., & Deming, D. 2005, ApJ, 632, 1122
- Sing, D. K., & López-Morales, M. 2009, A&A, 493, L31
- Snellen, I. A. G., & Covino, E. 2007, MNRAS, 375, 307
- Snellen, I. A. G., de Mooij, E. J. W., & Albrecht, S. 2009a, Nature, 459, 543
- Snellen, I. A. G., de Mooij, E. J. W., & Burrows, A. 2009b, ArXiv e-prints
- Sudarsky, D., Burrows, A., & Hubeny, I. 2003, ApJ, 588, 1121
- Todorov, K., Deming, D., Harrington, J., Stevenson, K. B., Bowman, W. C., Nymeyer, S., Fortney, J. J., & Bakos, G. A. 2010, ApJ, 708, 498
- Werner, M. W. et al. 2004, ApJS, 154, 1
- Zahnle, K., Marley, M. S., Freedman, R. S., Lodders, K., & Fortney, J. J. 2009, ApJ, 701, L20